Anatomy of Adsorption in Open-End and Closed-End Slit Mesopores: Adsorption, Desorption, and Equilibrium Branches of Hysteresis Loop

ARTICLE *in* THE JOURNAL OF PHYSICAL CHEMISTRY C · NOVEMBER 2014

Impact Factor: 4.77 · DOI: 10.1021/jp507600s

4 AUTHORS:

Yonghong Zeng
University of Queensland
14 PUBLICATIONS **64** CITATIONS
SEE PROFILE

Poomiwat Phadungbut
Suranaree University of Technology
9 PUBLICATIONS **9** CITATIONS
SEE PROFILE

Duong Do
University of Queensland
493 PUBLICATIONS **9,805** CITATIONS
SEE PROFILE

David Nicholson
University of Queensland
294 PUBLICATIONS **4,489** CITATIONS
SEE PROFILE

THE JOURNAL OF PHYSICAL CHEMISTRY C

Article

pubs.acs.org/JPCC

Anatomy of Adsorption in Open-End and Closed-End Slit Mesopores: Adsorption, Desorption, and Equilibrium Branches of Hysteresis Loop

Yonghong Zeng,[†] Poomiwat Phadungbut,[†,‡] D. D. Do,*[,†] and D. Nicholson[†]

[†]School of Chemical Engineering, The University of Queensland, St. Lucia, Queensland 4072, Australia

[‡]School of Chemical Engineering, Suranaree University of Technology, Nakhon Ratchasima 30000, Thailand

Supporting Information

ABSTRACT: We present a detailed analysis, using simulated data, of the adsorption and desorption in two finite length slit mesopores, one with both ends open to the surroundings and the other with one end closed, to investigate the microscopic behavior of an adsorbate in a confined space. The mesoscopic analysis of the interface separating the gas-like phase and the condensed phase reveals the mechanisms that lead to hysteresis in these two types of pore. The effects of pore width, temperature, and surface strength on these mechanisms are also studied to probe the detailed behavior of the system just before condensation and just after evaporation. In particular, for closed-end pores, we observe the development of a meniscus and the subsequent movement of the developed meniscus in adsorption and desorption. From these observations we are able to explain why adsorption and desorption branches have two distinct sections, slow and fast variations with pressure (corresponding to the two stages (1) developing meniscus and (2) developed meniscus), which have not been recognized in earlier literature.

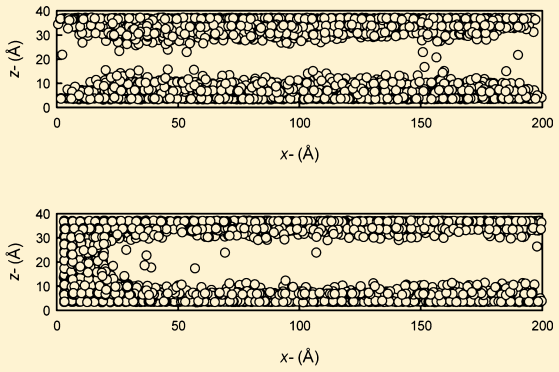

1. INTRODUCTION

The physics of a fluid in the confined space of a mesopore differs significantly from that of the corresponding bulk fluid, and understanding this physics helps to correlate the behavior of the condensed fluid with pore structure and hence to improve the characterization of the physical structure of porous solids. Unlike adsorption in micropores, where the adsorption isotherm is reversible because the filling and emptying of adsorbate follow the same path, the adsorption isotherm for open-end mesopores exhibits a hysteresis loop at temperatures less than the critical hysteresis temperature (T_{ch}), which is a function of adsorbate and pore dimensions.[1−3] Most theoretical studies of hysteresis focus on cylindrical pores, where the adsorption and desorption follow different paths because of the different curvatures of the interface separating the gas-like phase and the adsorbed phase, cylindrical for adsorption and hemispherical for desorption, giving rise to hysteresis as postulated by Cohan.[4] By this argument hysteresis would be absent in closed end cylindrical pores with only one end connected to the gas surroundings, because the interface is hemispherical for both adsorption and desorption. However, our recent comprehensive molecular simulation studies[5−7] have suggested that hysteresis can occur in both closed-end cylindrical and closed-end slit pores because the structure of the adsorbate is changing with the progress of adsorption, a feature that cannot be accounted for by the simple theory of Cohan. Hysteresis in closed-end pores has been reported experimentally[8−10] and supported by other simulation studies.[11−13]

According to simple thermodynamic theory, adsorbate would not condense in open-end slit pores because the radius of curvature of the growing adsorbate phase is infinity at the planar interface, and this has led some authors to aver that adsorbate layers must grow, in the same way as on a nonporous surface, until the pore is filled.[14] Desorption would then be controlled by the cylindrical meniscus formed at the pore mouth. This argument is now known to be incorrect because it does not account for the undulations that develop at the interface between the dense adsorbate phase and the contingent rarefied phase. The amplitude of these undulations increases at higher temperature, and the close approach of their maxima gives rise to condensation in slit pores.[15] In closed-end slit pores, the classical thermodynamic theory predicts that the isotherm is reversible because, as for cylindrical pores, the meniscus (although cylindrical not hemispherical) has the same shape during desorption as during adsorption, a conjecture refuted by our recent computer simulation studies.[5,16] The explanation is essentially the same as that given earlier for cylinders: that the structure of the adsorbate changes continuously with adsorption.

Received: July 28, 2014
Revised: October 10, 2014
Published: October 14, 2014

In this paper we report systematic computer simulations of fluids confined in slit mesopores of finite length with either both ends open or one end closed to the surrounding adsorptive. Pores with finite lengths have recently been revisited by Jagiello and Olivier,[17] who studied a model constructed from parallel circular graphene sheets, and finite pores having walls composed of carbon atoms have been studied by Lucena et al.[18] Our specific aim here is to dissect the isotherm and provide microscopic details of each stage of the adsorption and desorption processes at each pressure and loading. We place a particular emphasis on the pressures where condensation and evaporation take place, and their variation with pore size and temperature. In the case of isotherms where hysteresis occurs, it is known that portions of the loop are metastable, and it is of particular interest to determine the location of the equilibrium transition and to address a common question that arises frequently in the literature, namely, "which hysteresis branch is closer to equilibrium?" The results derived from this work will form a basis for an improved interpretation of experimental data in relation to the structure of a porous solid.

2. THEORY

2.1. Potential Models. We used argon as the model adsorbate, and its intermolecular interaction potential energy is described by the 12−6 Lennard-Jones (LJ) equation with σ_{ff} = 0.3405 nm and ε_{FF}/k_B = 119.8 K.

The two finite-length slit pore models are illustrated schematically in Figure 1. The pore length in the x-direction was 20 nm, and the dimension in the y-direction was 10 times the collision diameter of argon, σ_{ff}. The bulk reservoirs (gray region in Figure 1) were 3 nm long in the x-direction. The pore wall, consisting of three homogeneous graphene layers, was finite in the x-direction and infinite in the y-direction, and the solid−fluid (SF) interaction was modeled by the Bojan−Steele (BS) potential.[19−21] The molecular parameters for a carbon atom in a graphene layer are σ_{ss} = 0.34 nm, ε_{ss}/k_B = 28 K, and the surface density of a layer is ρ_s = 38.2 nm^{-2}.

2.2. Monte Carlo Scheme. In the grand canonical ensemble (GCMC) simulations, we used 200 000 cycles in the equilibration stage and the same number of cycles for the sampling stage. Each cycle consisted of 1000 displacement moves and insertions or deletions with equal probability, giving a total of 2 × 10^8 configurations. We note that this is at least 1 order of magnitude greater than would be used in typical MC runs in this type of system. In the equilibration stage, the maximum displacement length was initially set as half of the largest dimension of the simulation box and was adjusted at the end of each cycle to give an acceptance ratio of 20%.[22] The final maximum displacement attained at the end of the equilibration stage was then kept constant and used in the sampling stage.

The equilibrium transition in this paper was determined by the mid-density scheme, details of which can be found elsewhere.[23,24]

2.3. Analysis. The absolute pore density is defined as the number of particles per unit accessible volume, calculated from the equation

$$\rho = \langle N \rangle / V_{acc} \quad (1)$$

where $\langle N \rangle$ is the ensemble average of the number of particles in the pore and V_{acc} is the accessible volume where the SF potential is nonpositive.

The surface excess density is defined as the excess above a reference amount, given by

$$\Gamma_{ex} = \langle N_{ex} \rangle / A = [\langle N \rangle - V_{acc}\rho_b]/A \quad (2)$$

where ρ_b is the bulk density and A is the surface area of the solid.

The 2D-density distribution is defined as the local density of a two-dimensional bin

$$\rho(z, x) = \langle \Delta N(z, x) \rangle / [L_x \Delta z \Delta x] \quad (3)$$

where $\Delta N(z,x)$ is the number of particles in the bin bounded by $[z, z + \Delta z]$ and $[x, x + \Delta x]$. Bin size in both directions was $\Delta z = \Delta x = 0.1\sigma_{ff}$. The distribution curves were smoothed by averaging the density over a sphere of $0.5\sigma_{ff}$ radius. The gas−liquid interface was defined as a mathematical boundary between the gas phase and adsorbed phase, the density of which is 4 kmol/m^3 for argon at 87 K.

3. RESULTS AND DISCUSSION

3.1. Adsorption in Open-End and Closed-End Pores. The adsorption isotherms for argon at 87 K in the open-end and closed-end pores of 4 nm width and 20 nm length are shown in Figures 2 and 3, respectively. These isotherms will be used as a reference for our subsequent discussion of pores of different sizes and adsorption at temperatures other than 87 K.

A number of points, which may not have been widely recognized, are listed below:

1. There is hysteresis in both open- and closed-end pores, but the loop for the open-end pore is significantly larger.
2. The change in density on adsorption is vertical in the open-end pore, but, although sharp, it is not vertical in the closed-end pore.
3. The onset of condensation for the open-end pore (point C) occurs at a higher pressure than the for corresponding closed-end pore, and the pore density just before the jump is also higher.
4. The adsorbed density just before condensation is always higher than that just after evaporation for both open-end and closed-end pores. This is referred to as delayed condensation in the literature[26] because the condensation occurs at a pressure higher than the equilibrium pressure.
5. Both desorption boundaries for the open-end and closed-end pores have a knee (from F to G) just before evaporation.

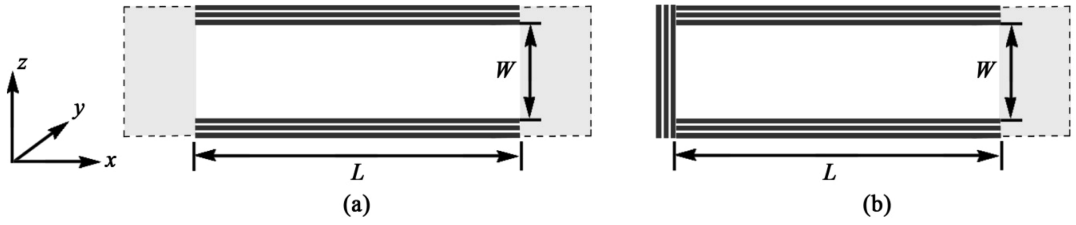

Figure 1. Schematic diagrams of the two pore models: (a) open-end pore; (b) closed-end pore. Bulk gas regions are shown as the gray area. Periodic boundary conditions are applied in the y-direction.

dx.doi.org/10.1021/jp507600s | J. Phys. Chem. C 2014, 118, 25496−25504

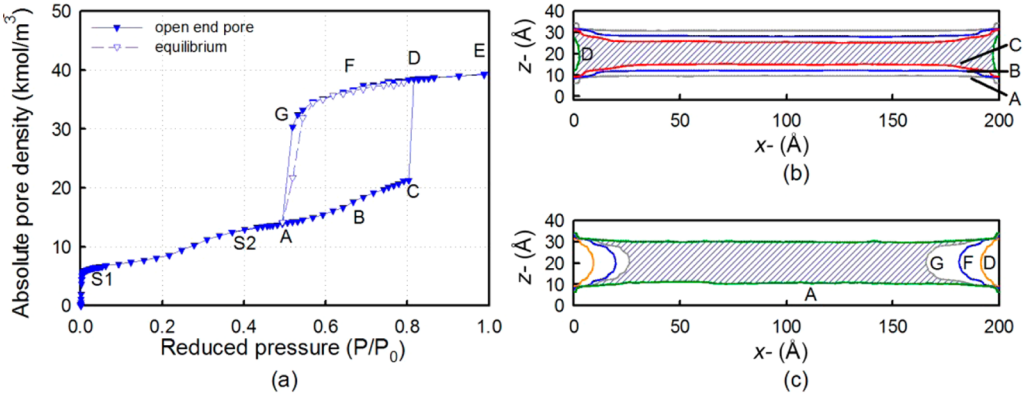

Figure 2. (a) Adsorption isotherm of argon at 87 K in an open-end pore of 4 nm width and 20 nm length. The open symbols and dashed lines represent equilibrium transitions. The saturation vapor pressure is calculated from a correlation.[25] Panels b and c are stages in the evolution of the vapor−liquid interface for adsorption and desorption, respectively. The points are marked on the isotherm in panel a.

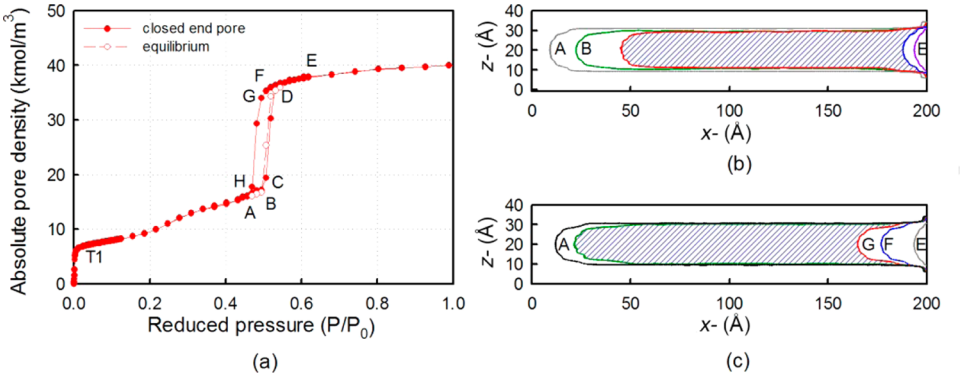

Figure 3. (a) Adsorption isotherm of argon at 87 K in a closed-end pore of 4 nm width and 20 nm length. The open symbols and dashed lines represent equilibrium transitions. Panels b and c are stages in the evolution of the vapor−liquid interface for adsorption and desorption, respectively. The points are marked on the isotherm in panel a.

6. The equilibrium transitions (dashed line) are second order for both open- and closed-end pores,[27] in contrast to the first-order transitions in pores of infinite length.[23,24,28] The equilibrium branch is closer to the desorption branch for the open-end pore but to the adsorption branch for the closed-end pore.

To understand the underlying microscopic reasons for the above observations, we studied the mesoscopic configuration of the adsorbate. Panels b and c of Figure 2 show the evolution with pressure of the interface separating the gas-like phase and the adsorbed phase in the open-end and closed-end pores, respectively. These interfaces were obtained from contours of the smoothed average 2D density distributions.

3.1.1. Adsorption in the Open-End Pore. Molecular layering occurs on the pore walls up to point A, beyond which the adsorbed layer is metastable up to the condensation pressure (which is why the condensation is referred to as delayed condensation). As the pressure is increased, the two opposing interfaces approach each other, and at point C condensation occurs, because fluctuations at the interfaces initiate the formation of a concave liquid bridge.[15] This precipitates an instant condensation of liquid-like adsorbate with menisci that extend to the pore mouth (point D). The amount associated with this instant filling is shown as the shaded region in Figure 2b. Further increase in pressure fills the regions near the pore mouths, and the curvature of the menisci approach zero as the pressure approaches the saturation vapor pressure.

3.1.2. Desorption in the Open-End Pore. Desorption from the filled pore begins with the formation of two menisci at the pore mouth; as the pressure is decreased, the menisci recede into the pore interior, and there is an evolution in the shape of the meniscus in which the radii of curvature decrease from points E to G. We refer to this range as one where the interface is developing; at point G the interface has developed such that any further decrease in pressure would lead to a larger radius of curvature, which is not possible because a larger radius of curvature is possible only at a higher pressure. Therefore, the adsorbate density along the desorption branch undergoes a sharp decrease with pressure, and complete evaporation of the condensed fluid has occurred at point A. It is commonly thought that the liquid bridge evaporates only when it becomes a very thin biconcave lens, but this is not correct as shown in Figure 2c, where it is clear that the evaporation occurs when the liquid bridge is still very thick and evaporation takes place because the interface is fully developed; any further decrease in pressure would lead to a larger radius of curvature, and therefore instant evaporation is the only possibility at pressures below point G. The amount associated with instant evaporation is shown as the shaded region in Figure 2c, which is quantitatively different from the one at condensation (shaded region in Figure 2b). This interesting point does not seem to have been recognized in previous literature. Just after evaporation (point A), the adsorbed layer is thinner than it was just before condensation, which further confirms our

dx.doi.org/10.1021/jp507600s | J. Phys. Chem. C 2014, 118, 25496−25504

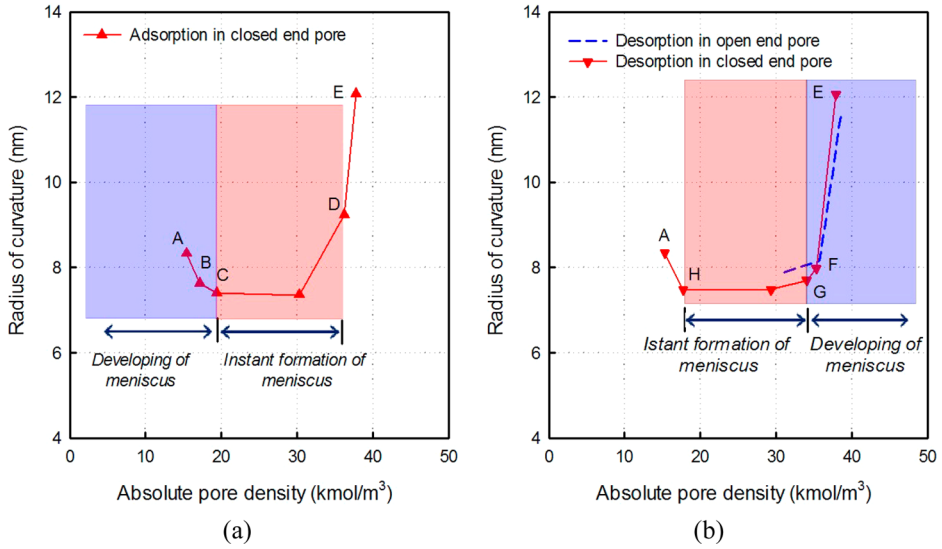

Figure 4. Radius of curvature of the cylindrical meniscus in the closed-end pore: (a) adsorption; (b) desorption. The labels correspond to those in Figures 2 and 3.

assertion that the adsorbed layer along the adsorption branch is metastable.

Our recent study[5,16] has proved that the classical thermodynamic theory of Kelvin and Cohan is invalid for the description of pore filling and emptying in a closed-end pore, because the condensed fluid in the confined space is not the same as that in the corresponding bulk liquid. Here, we extended this work to analyze more fully the difference in the evolution of the radius of curvature of the meniscus by image analysis, as shown in Figure 4.

3.1.3. Adsorption in the Closed-End Pore. During the initial stage of adsorption (up to point A), molecular layering occurs on the pore walls and at the closed end, and the meniscus starts to form at the closed end and develops as pressure is increased. To facilitate the discussion, we identify the two regions shown in Figure 5: (1) the condensed fluid adjacent to the closed end

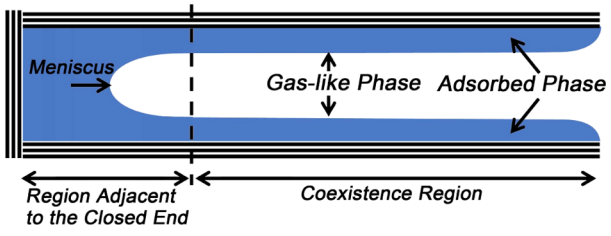

Figure 5. Schematic of the closed-end pore (to simplify the diagram we illustrate the coexistence region without an undulating surface).

and (2) the coexistence region of the adsorbed phase and the gas-like phase.

The curvature of the interface in the first region is cylindrical and in the latter is infinity. As pressure is increased from point A, the radius of the cylindrical interface decreases (i.e., the curvature increases), as shown in Figure 4a, up to point C. During this development, the thickness of the adsorbed layer in the coexistence region becomes slightly thicker because molecules prefer the stronger adsorption field, due to the presence of more neighboring molecules at closer distance, at the cylindrical interface. Once the cylindrical interface is fully developed at point C, any further increase in pressure would result in a further decrease in the radius of curvature, which would trigger a sharp condensation up to point D, where the cylindrical interface is close to the pore mouth and its radius of curvature increases. We refer to the region before point C as the region of developing cylindrical interface (shown as the blue-shaded region in Figure 4a), and the region after point C as the region of fast movement of the developed interface (shown as the red-shaded region). It is noted that the thickness of the adsorbed layer in the coexistence region just before condensation (point C) is much less than that in the open-end pore (point C) and occurs at a lower pressure. The reason for this earlier condensation is the advance of the meniscus from the closed end, compared to the open-end pore, where there is no nucleation of the meniscus.

3.1.4. Desorption from the Closed-End Pore. As pressure is reduced in the filled pore, a meniscus is formed at the pore mouth, and the resulting meniscus develops from point E to point G (the blue region in Figure 4b), with a radius of curvature decreasing in the same manner as desorption from the open-end pore (shown as a dashed line). At point G, the meniscus is fully developed and reaches its minimum radius of curvature. As the pressure is further decreased, the radius of curvature of the meniscus becomes slightly larger, which leads to a rapid regression of the interface to the pore interior (the red region in Figure 4b). We especially note that the radii of curvature of the interface at the same pore density during adsorption and desorption are actually different, for example, at points D and F in Figure 4b. There are two reasons for this: (i) the average thickness of the adsorbed layers in the coexistence region is increased during adsorption but remains constant during desorption; (ii) the condensed fluid becomes more structured as adsorption progresses. Elsewhere, we have presented quantitative studies to support these assertions.[5,16] Comparison of the evolution of the meniscus in the open-end pore (dashed line in Figure 4b), where the minimum in the radius of curvature is the same, shows that the developing meniscus during desorption is the same for both pores. Another feature, which has not been described earlier, is that the thickness of the adsorbed layers in the coexistence region in the closed-end pore is the same as the thickness of the adsorbed layers just after evaporation in the open-end pore. This is

dx.doi.org/10.1021/jp507600s | J. Phys. Chem. C 2014, 118, 25496−25504

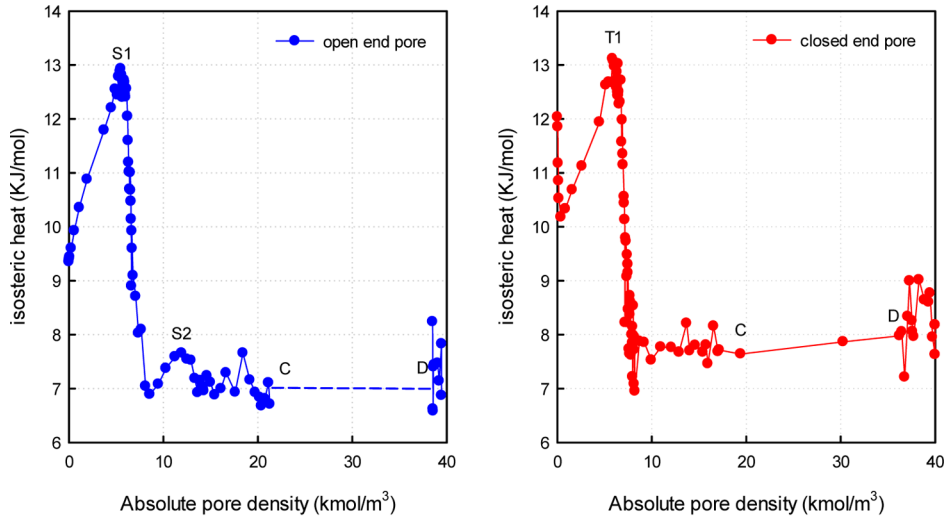

Figure 6. Isosteric heats of adsorption: (a) open-end pore; (b) closed-end pore.

consistent with the fact that the coexistence region in the closed-end pore is similar to that in the open-end pore.

Figure 6 shows the isosteric heats for argon adsorption in the open-end pore and the closed-end pore. The isosteric heat in the open-end pore initially increases almost linearly from zero loading to the monolayer coverage (Point S1 in Figure 6a), as a result of the increase in the number of neighboring molecules on the surface. Once the formation of the first layer is complete, the isosteric heat decreases sharply because the added molecules are farther away from the surface and therefore in a weaker adsorbent potential energy field. The second maximum (Point S2 in Figure 6a) corresponds to the densification of the second layer as the loading is increased. A further increase in pressure results in the formation of higher layers until condensation occurs at point C. Along the vertical condensation branch of the isotherm (CD), the isosteric heat is relatively constant (shown as a dashed line in Figure 6a) because of the compensation between the decrease in the solid–fluid interaction and the increase in the fluid–fluid interaction.[29] After the condensation, the isosteric heat increases sharply, due to the densification of the condensed fluid.

The isosteric heat at zero loading in the closed-end pore is 12 kJ/mol, in contrast to the open-end pore where the corresponding heat is only 9.5 kJ/mol. This enhancement is due to the strong potential exerted by the corners at the closed end. As loading is increased, the isosteric heat rapidly decreases as this high-energy region becomes saturated and new molecules adsorb on the pore walls to form a monolayer (up to point T1) and on the advancing meniscus at the closed end. The pattern of the heat curve through this stage is similar to that observed in the open-end pore. Interestingly, beyond the monolayer coverage (point T1) the isosteric heat for the closed-end pore is higher than that for the open-end pore, at the same loading, by about 0.5 kJ/mol. This is consistent with the mechanism proposed earlier for adsorption in a closed-end pore, where molecules adsorbing at the cylindrical interface are in a stronger potential energy field than they would be on a flat interface because there are more neighboring molecules at separations closer to the potential energy minimum. This means that the condensed fluid in the closed-end pore is more cohesive.

3.2. Effect of Pore Width. Figure 7 shows the effects of pore width on the adsorption isotherm and its hysteresis loop for the open-end pore (Figure 7a) and the closed-end pore (Figure 7b). The key features are noted below:

1. The adsorption boundary for both pores shifts to higher pressure as the pore width is increased. For the open-end pore, this is because more adsorbed layers are required before the gas-like core is small enough to induce the condensation. However, for the closed-end pore, more adsorbed layers are needed for the meniscus to fully develop before the developed meniscus can advance to the pore mouth.
2. The desorption boundary for both pores also shifts to higher pressure, which is due to the larger radius of curvature of the interfaces formed at the pore mouth.
3. For the 3 nm closed-end pore, the condensation does not merge with the desorption branch because of the continuing compression of the condensed adsorbate beyond condensation; upon desorption, the condensed adsorbate is more cohesive and does not desorb until a lower pressure is reached. This has also been observed for isotherms at lower temperatures.
4. The condensation in the 6 nm and larger open-end pores occurs at a pressure greater than the saturation vapor pressure because there is a delay in the nucleation of the liquid bridge formed from the metastable adsorbed layer. However, the pressure along the equilibrium branch (dashed line) is always less than the saturation vapor pressure, as should be the case.
5. For a given pore size, the equilibrium transitions for both pores are practically the same. This has not been previously recognized in the literature, and it is suggested that it is the metastable state of the adsorbate in the open-end pore that accounts for the difference between its isotherm and that of the closed-end pore.

The hysteresis loop can be further understood by studying the surface excess density just before condensation and just after evaporation as a function of pore size (as shown in Figure 8) for the open-end and closed-end pores. Our first observation for both pore types is that the surface densities just

dx.doi.org/10.1021/jp507600s | J. Phys. Chem. C 2014, 118, 25496–25504

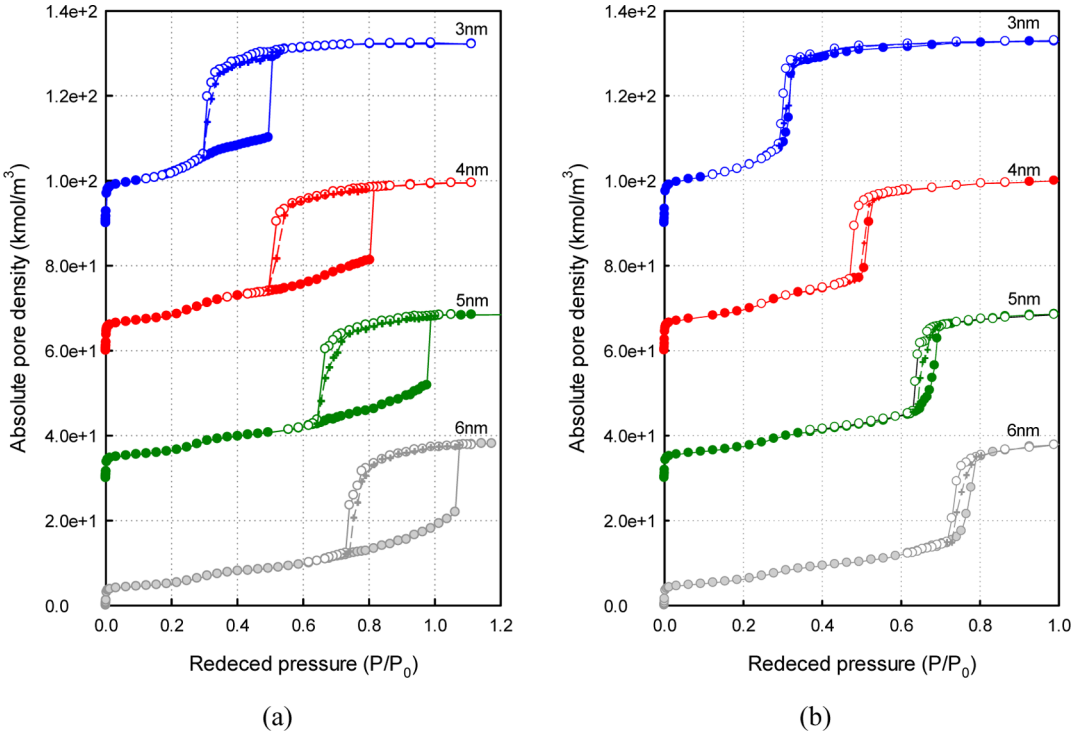

Figure 7. Isotherms for argon at 87 K in a pore of length 20 nm as a function of pore width: (a) open-end pore; (b) closed-end pore. Isotherms for 5, 4, and 3 nm are shifted up by 30, 60, and 90 kmol/m^3, respectively.

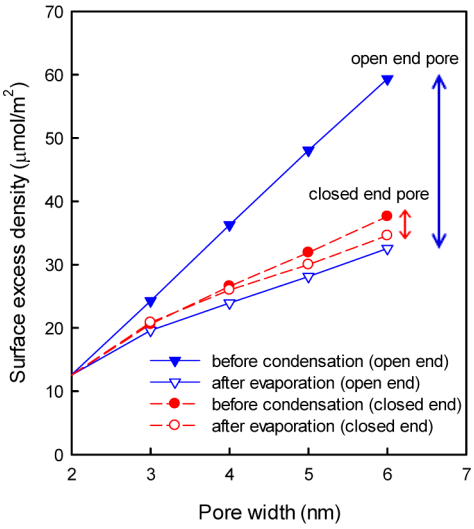

Figure 8. Effect of pore width on the surface excess density just before condensation and just after evaporation. Dashed lines are for the closed-end pore, whereas solid lines are for the open-end pore.

before condensation and just after evaporation are almost linearly dependent on pore size and intersect at 2 nm. This supports the traditional demarcation between micropore and mesopore of 2 nm for simple gases, with a molecular size similar to that of argon. Furthermore, the surface density at this intersection is about 12 μmol/m^2, which is the monolayer concentration of argon on a homogeneous flat surface. As the pore width is increased, the surface densities just before condensation for both pores increase in a linear manner. This is because more layers are required to reach the critical threshold separation distance between the two opposite adsorbed layers in the open-end pore,[15] whereas in the closed-end pore more layers are required for the meniscus to develop at the closed end. As a result, the adsorption branches shift to higher pressure for larger pores for both pore models. The increase in the surface density just before condensation is greater for the open-end pore, because no nucleation of a meniscus occurs during adsorption prior to condensation. This also explains why condensation occurs at a pressure greater than the saturation vapor pressure in the 6 nm and larger pores, as the separation distance between two opposite adsorbed layers just before condensation would be impossible to achieve at a pressure lower than P_0 in large open-end pores. The surface densities just after evaporation also increase in larger pores for both types of pores, and this is associated with the higher desorption pressure.

3.3. Effect of Temperature. Figure 9 shows the isotherms for pores of 4 nm width at various temperatures. The effect of temperature on the equilibrium transition and isotherm below the triple point has not been previously reported in the literature.

A number of interesting features may be noted:

1. For temperatures below the triple point (the 77 K isotherm), the adsorption branch and the desorption branch are still separated by a narrow gap just after condensation in both pores. This is due to the continued compression of the condensed fluid after condensation; this gap disappears as the temperature is increased.
2. When the temperature is increased, the vertical adsorption boundary of the hysteresis loop shifts to lower reduced pressures in the open-end pore, and the sharp adsorption boundary in the closed-end pore shifts to higher reduced pressures. This has not been noted previously in the literature. In the open-end pore, this is because the amplitude of the fluctuations at the adsorbate interface increases at higher temperatures, resulting in

dx.doi.org/10.1021/jp507600s | J. Phys. Chem. C 2014, 118, 25496−25504

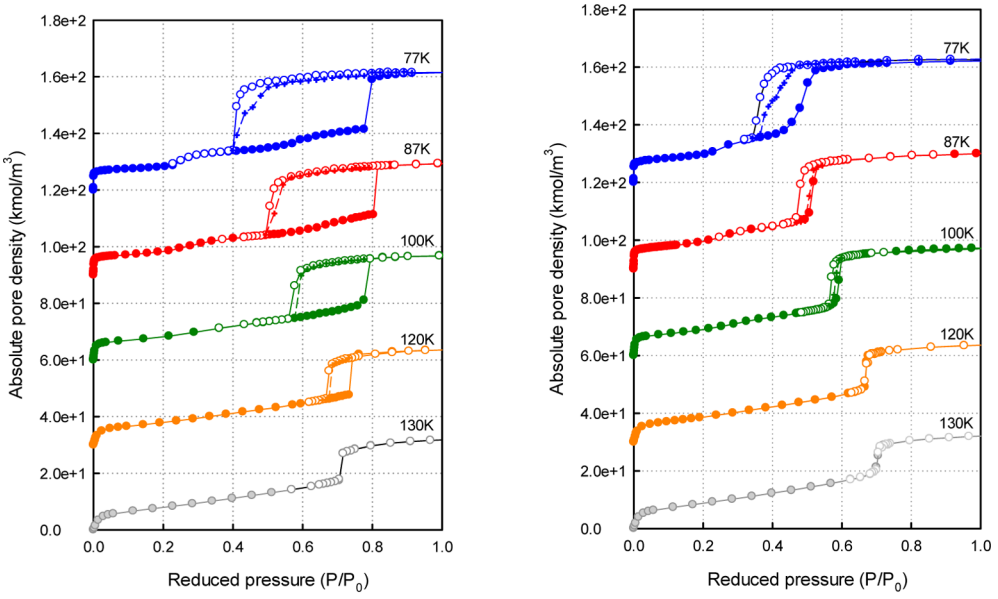

Figure 9. Isotherms for argon in slit pore of 4 nm width and 20 nm length as a function of temperature: (a) open-end pore; (b) closed-end pore. Isotherms for 120, 100, 87, and 77 K are shifted up by 30, 60, 90, and 120 kmol/m^3, respectively. Saturated pressures at different temperatures are calculated from correlation.[25]

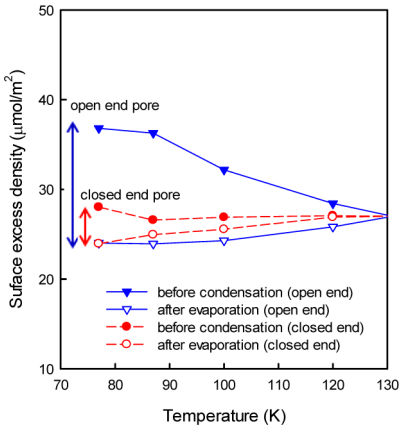

Figure 10. Effect of temperature on the surface excess just before condensation and just after evaporation.

condensation at a lower chemical potential (lower reduced pressure). In the closed-end pore, a higher pressure is needed for the meniscus to develop as the temperature is increased. However, condensation for different temperatures occurs at about the same *reduced* pressure for a 3 nm open-end pore (Figure S1 in the Supporting Information), whereas it shifts to higher reduced pressure for smaller pores (Figure S2). The different evolution of hysteresis with temperature is due to stabilization of the adsorbed layer in smaller pores.

3. The desorption boundary shifts to higher reduced pressures with temperature for both pore models, because the condensed fluid becomes less cohesive as the temperature is increased.
4. For this pore width (4 nm), hysteresis disappears at 120 K in the closed-end pore, whereas T_{ch} of the open-end pore is around 130 K. It should be noted that T_{ch} is pore width dependent but appears to reach a constant value for sufficiently large mesopores (>5 nm).[7]

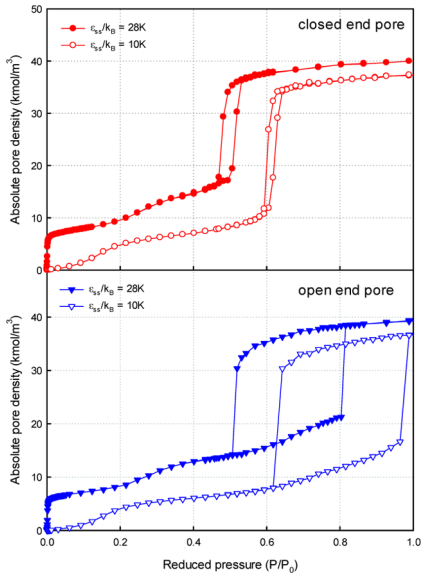

Figure 11. Isotherms for pores of 4 nm width and 20 nm length with different pore affinities, 28K and 10K, respectively.

5. The equilibrium branch (dashed line) shifts to higher reduced pressures for both pore models. It is closer to the desorption branch for the open-end pore, but is closer to the adsorption branch for the closed-end pore, except at 77 K. At this temperature, the equilibrium transitions in both pore models occur in stages; this could be due to a change in the structure of the adsorbed phase at temperatures below the triple point of argon. Further investigations are required to substantiate this point.

The changes with temperature, of the surface excess density (μmol/m^2), at points just before condensation and just after evaporation are summarized in Figure 10 for the two pore models. At the lowest temperature studied (77 K), the surface

dx.doi.org/10.1021/jp507600s | J. Phys. Chem. C 2014, 118, 25496−25504

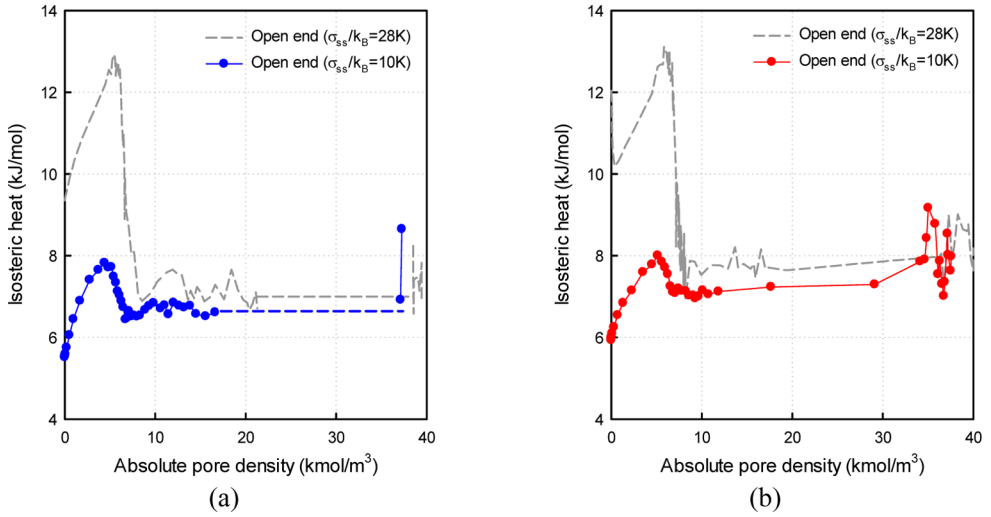

Figure 12. Isosteric heats of adsorption in pore with 10K affinity: (a) open-end pore; (b) closed-end pore. Dashed line is the heat of evaporation from GEMC.[30]

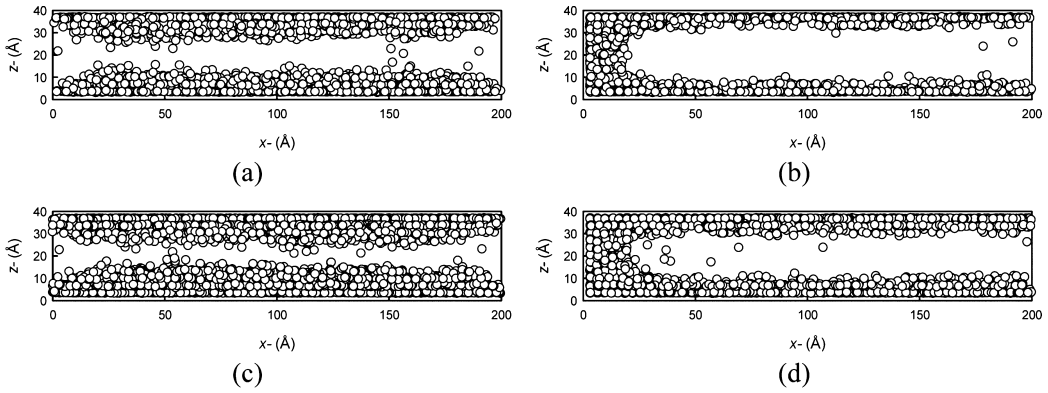

Figure 13. Snapshots of adsorbed argon at 87 K just before condensation in pores of 4 nm width and 20 nm length with different surface affinities: (a, b) σ_{ss}/k_B = 10K; (c, d) σ_{ss}/k_B = 28K.

density just before condensation is higher in both pore models than at higher temperatures, but is lower just after evaporation. This is because the condensed adsorbate at 77 K is much denser (and closer to a solid-like structure). As the temperature is increased, the surface densities just before condensation decrease, whereas those just after evaporation increase slightly. The plots in Figure 10 intersect at T_{ch}. The critical hysteresis temperature is a consequence of the competition between two mechanisms: thermal fluctuations and the formation and movement of interfaces. When temperature is increased, undulations develop at the adsorbate interface, which also becomes more diffuse, due to thermal fluctuations, and both factors facilitate the formation of a liquid bridge embryo.[7] This is why the surface excess density before condensation in the open-end pore decreases significantly at higher temperature. At temperatures above T_{ch}, adsorption and desorption in both pore models will be dominated by thermal fluctuations and hysteresis disappears.

3.4. Effect of Surface Strength. The effects of surface strength are shown in Figure 11 for argon adsorption at 87 K. For the case of a weaker 10K pore, the isotherms of both pores shift to higher pressure, compared to the graphite 28K surface, because of the weaker SF interaction. It is interesting to note that the width of the hysteresis loop remains constant for the open-end pores and is smaller for the weaker closed-end pore. This indicates that the existence of hysteresis can be attributed to the metastability of condensate, irrespective of the surface strength.

The isosteric heat of adsorption in the weak 10K pores is shown in Figure 12, where we see the suppression of the heat, compared to the stronger 28K pores. The suppression is noted at zero loading.

It is interesting to observe from Figure 11 that the adsorbed density just before condensation is lower for weaker pores. To explain this, we present snapshots of argon molecules just before condensation in Figure 13. For the weaker 10K open-end pore, the undulation of the interfaces is greater because there is less stabilization by the surface, and therefore the formation of a liquid embryo is possible at a lower density. The same reasoning applies for the case of the weaker 10K closed-end pore, where lower stabilization by the surface results in the development of the undulating surface at a lower density.

4. CONCLUSIONS

We have presented a detailed simulation study of argon adsorption in open-end and closed-end slit mesopores. The mechanisms of hysteresis in these two pore models are explained by mesoscopic analysis, and effects of pore width, temperature, and surface strength on hysteresis are also studied. Through a detailed comparison between the open-end and closed-end

dx.doi.org/10.1021/jp507600s | J. Phys. Chem. C 2014, 118, 25496−25504

pores, it was found that (1) the evolution of the interface between a gas-like phase and an adsorbate (condensed) phase is further evidence confirming the existence of hysteresis in both open-end and closed-end pores; (2) the isosteric heat at zero loading in a closed-end pore is higher than that in an open-end pore due to the lower potential energy at the closed end, where there is overlap of interactions from adjacent surfaces; (3) the surface excess density just before condensation in both types of pore is linearly dependent on pore size and is greater in open-end pores because of the absence of nucleation during adsorption; (4) the surface excess just before condensation in open-end pores decreases significantly with temperature due to thermal fluctuation; (5) hysteresis loops are also observed for both pore types when the adsorbent has a weaker affinity.

■ ASSOCIATED CONTENT

Supporting Information

Figures S1 and S2. This material is available free of charge via the Internet at http://pubs.acs.org.

■ AUTHOR INFORMATION

Corresponding Author

*(D.D.D.) E-mail: d.d.do@uq.edu.au.

Notes

The authors declare no competing financial interest.

■ ACKNOWLEDGMENTS

This project is supported by the Australian Research Council.

■ REFERENCES

(1) Thommes, M. Physical Adsorption Characterization of Ordered and Amorphous Mesoporous Materials. In *Nanoporous Materials, Science and Engineering*; Lu, G., Zhao, X. S., Eds.; Imperial College Press, London, UK, 2004; Vol. 4, 317−364.

(2) Everett, D. H.; Haynes, J. M. Capillarity and Porous Materials: Equilibrium Properties. *Colloid Sci.* **1973**, 123−172.

(3) Horikawa, T.; Do, D. D.; Nicholson, D. Capillary Condensation of Adsorbates in Porous Materials. *Adv. Colloid Interface* **2011**, *169*, 40−58.

(4) Cohan, L. H. Sorption Hysteresis and the Vapor Pressure of Concave Surfaces. *J. Am. Chem. Soc.* **1938**, *60*, 433−435.

(5) Nguyen, P. T. M.; Do, D. D.; Nicholson, D. On the Irreversibility of the Adsorption Isotherm in a Closed-End Pore. *Langmuir* **2013**, *29*, 2927−2934.

(6) Fan, C.; Do, D. D.; Nicholson, D. On the Existence of a Hysteresis Loop in Open and Closed End Pores. *Mol. Simul.* **2014**, 1−11.

(7) Zeng, Y.; Fan, C.; Do, D. D.; Nicholson, D. Condensation and Evaporation in Slit-Shaped Pores: Effects of Adsorbate Layer Structure and Temperature. *J. Phys. Chem. B* **2014**, *118*, 3172−3180.

(8) Coasne, B.; Grosman, A.; Ortega, C.; Simon, M. Adsorption in Noninterconnected Pores Open at One or at Both Ends: A Reconsideration of the Origin of the Hysteresis Phenomenon. *Phys. Rev. Lett.* **2002**, *88*, 256102-1−256102-4.

(9) Wallacher, D.; Künzner, N.; Kovalev, D.; Knorr, N.; Knorr, K. Capillary Condensation in Linear Mesopores of Different Shape. *Phys. Rev. Lett.* **2004**, *92*, 195704-1−195704-4.

(10) Bruschi, L.; Fois, G.; Mistura, G.; Sklarek, K.; Hillebrand, R.; Steinhart, M.; Gösele, U. Adsorption Hysteresis in Self-Ordered Nanoporous Alumina. *Langmuir* **2008**, *24*, 10936−10941.

(11) Ancilotto, F.; Da Re, M.; Grubišić, S.; Hernando, A.; Silvestrelli, P. L.; Toigo, F. Grand Canonical Monte Carlo Study of Argon Adsorption in Aluminium Nanopores. *Mol. Phys.* **2011**, *109*, 2787−2796.

(12) Puibasset, J. Monte-Carlo Multiscale Simulation Study of Argon Adsorption/Desorption Hysteresis in Mesoporous Heterogeneous Tubular Pores Like MCM-41 or Oxidized Porous Silicon. *Langmuir* **2009**, *25*, 903−911.

(13) Bruschi, L.; Mistura, G.; Liu, L.; Lee, W.; Gösele, U.; Coasne, B. Capillary Condensation and Evaporation in Alumina Nanopores with Controlled Modulations. *Langmuir* **2010**, *26*, 11894−11898.

(14) Brunauer, S.; Deming, L. S.; Deming, W. E.; Teller, E. On a Theory of the Van Der Waals Adsorption of Gases. *J. Am. Chem. Soc.* **1940**, *62*, 1723−1732.

(15) Fan, C.; Zeng, Y.; Do, D. D.; Nicholson, D. An Undulation Theory for Condensation in Open End Slit Pores: Critical Hysteresis Temperature & Critical Hysteresis Pore Size. *Phys. Chem. Chem. Phys.* **2014**, *16*, 12362−12373.

(16) Fan, C.; Do, D. D.; Nicholson, D. On the Hysteresis of Argon Adsorption in a Uniform Closed End Slit Pore. *J. Colloid Interface Sci.* **2013**, *405*, 201−210.

(17) Jagiello, J.; Olivier, J. P. A Simple Two-Dimensional NLDFT Model of Gas Adsorption in Finite Carbon Pores. Application to Pore Structure Analysis. *J. Phys. Chem. B* **2009**, *113*, 19382−19385.

(18) Lucena, S. M. P.; Paiva, C. A. S.; Silvino, P. F. G.; Azevedo, D. C. S.; Cavalcante, C. L., Jr. The Effect of Heterogeneity in the Randomly Etched Graphite Model for Carbon Pore Size Characterization. *Carbon* **2010**, *48*, 2554−2565.

(19) Bojan, M. J.; Steele, W. A. Computer Simulation of Physisorption on a Heterogeneous Surface. *Surf. Sci.* **1988**, *199*, L395−L402.

(20) Bojan, M. J.; Steele, W. A. Computer Simulations of the Adsorption of Xenon on Stepped Surfaces. *Mol. Phys.* **1998**, *95*, 431 −437.

(21) Bojan, M. J.; Steele, W. A. Computer Simulation of Physical Adsorption on Stepped Surfaces. *Langmuir* **1993**, *9*, 2569−2575.

(22) Mountain, R. D.; Thirumalai, D. Quantative Measure of Efficiency of Monte Carlo Simulations. *Physica A* **1994**, *210*, 453−460.

(23) Liu, Z.; Herrera, L.; Nguyen, V. T.; Do, D. D.; Nicholson, D. A Monte Carlo Scheme Based on Mid-Density in a Hysteresis Loop to Determine Equilibrium Phase Transition. *Mol. Simul.* **2011**, *37*, 932−939.

(24) Liu, Z.; Do, D. D.; Nicholson, D. A Thermodynamic Study of the Mid-Density Scheme to Determine the Equilibrium Phase Transition in Cylindrical Pores. *Mol. Simul.* **2011**, *38*, 189−199.

(25) Lotfi, A.; Vrabec, J.; Fischer, J. Vapour Liquid Equilibria of the Lennard-Jones Fluid from the Npt Plus Test Particle Method. *Mol. Phys.* **1992**, *76*, 1319−1333.

(26) Cordero, S.; Rojas, F.; Kornhauser, I.; Esparza, M. Menisci Interactions During Adsorption on Mesoporous Materials: Evaluation of Delayed and Advanced Adsorption. *Adsorption* **2005**, *11*, 91−96.

(27) Klomkliang, N.; Do, D. D.; Nicholson, D. On the Hysteresis Loop and Equilibrium Transition in Slit-Shaped Ink-Bottle Pores. *Adsorption* **2013**, *19*, 1273−1290.

(28) Jorge, M.; Seaton, N. A. Molecular Simulation of Phase Coexistence in Adsorption in Porous Solids. *Mol. Phys.* **2002**, *100*, 3803−3815.

(29) Wang, Y.; Do, D. D.; Nicholson, D. Study of Heat of Adsorption across the Capillary Condensation in Cylindrical Pores. *Colloid Surf. A* **2011**, *380*, 66−78.

(30) Nguyen, V. T.; Do, D. D.; Nicholson, D.; Ustinov, E. A. Application of the Kinetic Monte Carlo Method in the Microscopic Description of Argon Adsorption on Graphite. *Mol. Phys.* **2012**, *110*, 2281−2294.